Supporting Information

For

Preparation and Controlled Degradation of Model Amphiphilic Long-Subchain Hyperbranched Copolymers: Hyperblock versus Hypergraft

Jinxian Yang,[1,2] Yixia Li,[1] Nairong Hao,[1] Ahmad Umair,[1] Anhong Liu,[1] Lianwei Li,[1,*] and Xiaodong Ye[1,3,*]

1) *Hefei National Laboratory for Physical Sciences at the Microscale, Department of Chemical Physics, University of Science and Technology of China, Hefei, Anhui 230026, China*

2) *Shenzhen Key Laboratory for Functional Polymer, School of Chemistry and Chemical Engineering, Shenzhen University, Shenzhen, Guangdong 518060, China*

3) *CAS Key Laboratory of Soft Matter Chemistry, University of Science and Technology of China, Hefei, Anhui 230026, P. R. China*

*To whom correspondence should be addressed: xdye@ustc.edu.cn and llw@mail.ustc.edu.cn

Table S1. Molar mass information from GPC and ^{1}H NMR.

		GPC			^{1}H NMR
	Samples	M_n/(g/mol)	M_w/(g/mol)	M_w/M_n	M_w/(g/mol)
For Hyperblock	PCL_{26}-OH-Br	3.4×10^3	4.8×10^3	1.41	3.3×10^3
	PCL_{26}-*b*-$PTEGMA_{12}$-$2N_3$	7.5×10^3	9.8×10^3	1.31	6.0×10^3
	HB-PCL_{26}-*b*-$PTEGMA_{12}$	3.54×10^4	1.22×10^5	3.45	-
For Hypergraft	$PTEGMA_{13}$	2.7×10^3	3.4×10^3	1.22	3.2×10^3
	PCL_{23}-$2N_3$	4.2×10^3	5.1×10^3	1.21	2.9×10^3
	HB-PCL_{23}	8.7×10^3	2.34×10^4	2.69	-
	HB-PCL_{23}-*g*-$PTEGMA_{13}$	5.47×10^4	9.32×10^4	1.70	-

Table S2. Molar mass information of the degradation products from GPC.

	Time/h	M_n/(g/mol)	M_w/(g/mol)	M_w/M_n
Fractionated HB-PCL_{26}-*b*-$PTEGMA_{12}$ in 10mM DTT	0	5.82×10^4	9.58×10^4	1.65
	30	1.10×10^4	1.61×10^4	1.45
Fractionated HB-PCL_{23}-*g*-$PTEGMA_{13}$ in 10mM DTT	0	5.47×10^4	9.32×10^4	1.70
	26	3.7×10^3	5.2×10^3	1.31

Table S3. Molar mass information of the fractioned hyperbranched copolymers used for SAs from GPC.

	GPC				
		Fractionated samples	M_n/(g/mol)	M_w/(g/mol)	M_w/M_n
For Hyperblock	With disulfide bonds	HB-PCL_{25}-*b*-$PTEGMA_6$	3.89×10^4	6.10×10^4	1.56
		HB-PCL_{26}-*b*-$PTEGMA_{12}$	5.82×10^4	9.58×10^4	1.65
		HB-PCL_{25}-*b*-$PTEGMA_{26}$	6.78×10^4	1.11×10^5	1.65
	Without disulfide	*R*-HB-PCL_{26}-*b*-$PTEGMA_{12}$	5.67×10^4	1.20×10^4	2.12
For Hypergraft	With disulfide bonds	HB-PCL_{23}-*g*-$PTEGMA_{13}$	5.47×10^4	9.32×10^4	1.70
		HB-PCL_{25}-*g*-$PTEGMA_{21}$	5.48×10^4	9.14×10^4	1.66
	Without disulfide	*R*-HB-PCL_{22}-*g*-$PTEGMA_{14}$	4.97×10^4	7.95×10^4	1.60

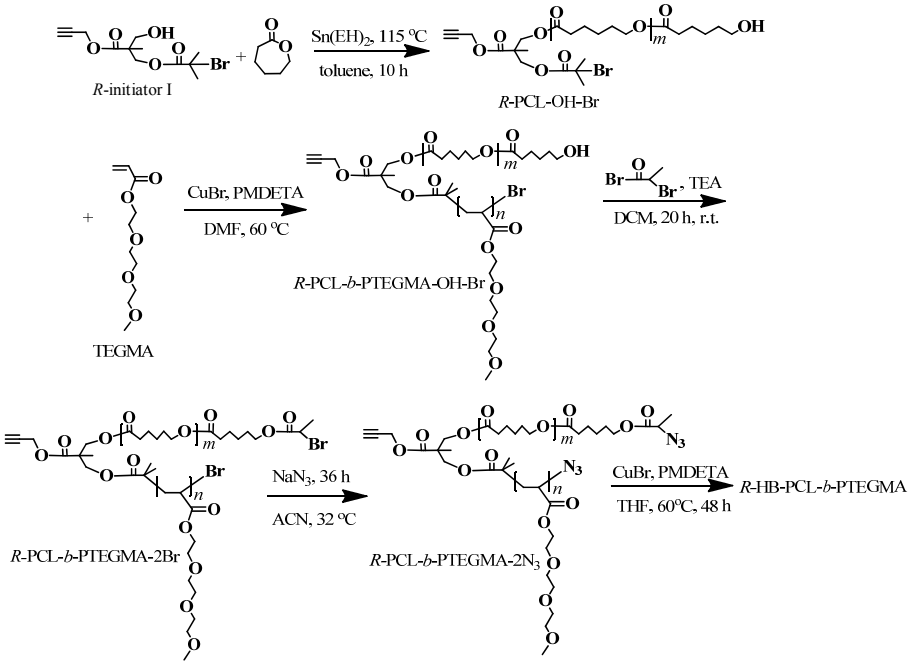

Scheme S1. Schematic illustration of the synthesis of reference sample *R*-HB-PCL-*b*-PTEGMA without disulfide linkages.

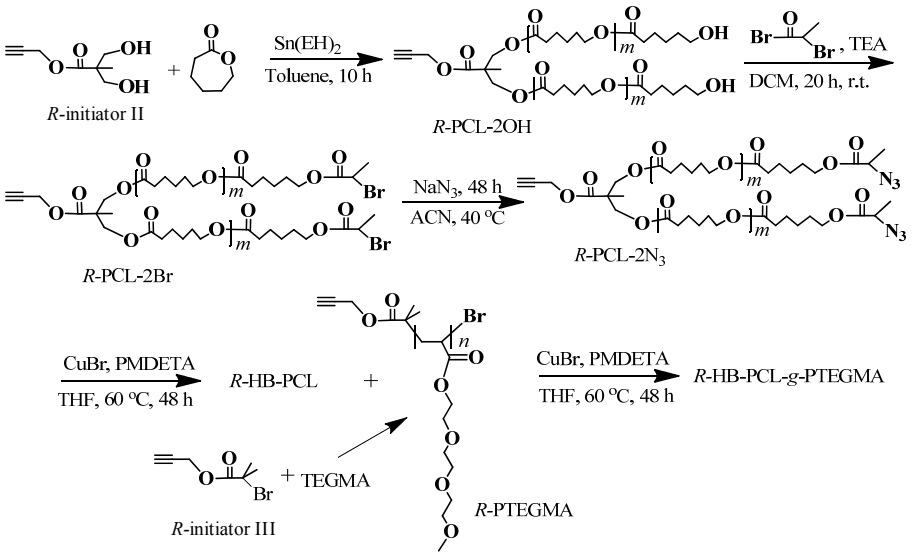

Scheme S2. Schematic illustration of the synthesis of reference sample *R*-HB-PCL-*g*-PTEGMA without disulfide linkages.

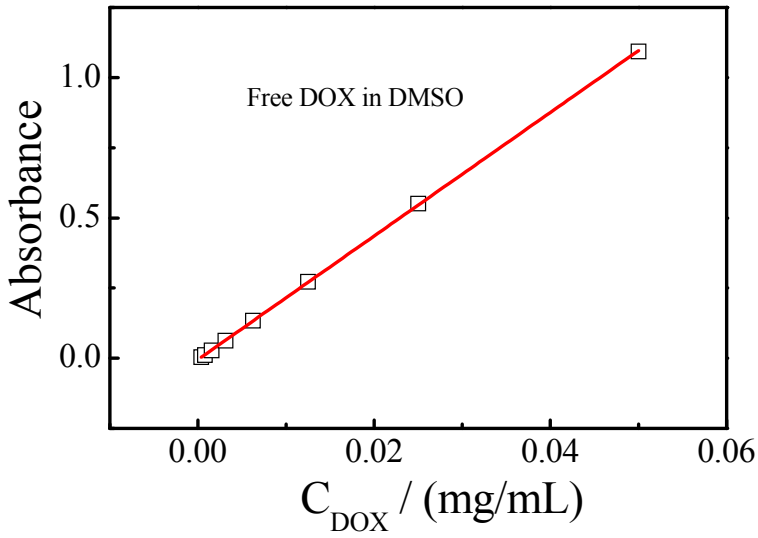

Figure S1. Standard curve of DOX in DMSO obtained by UV-vis spectrometer at 485 nm.

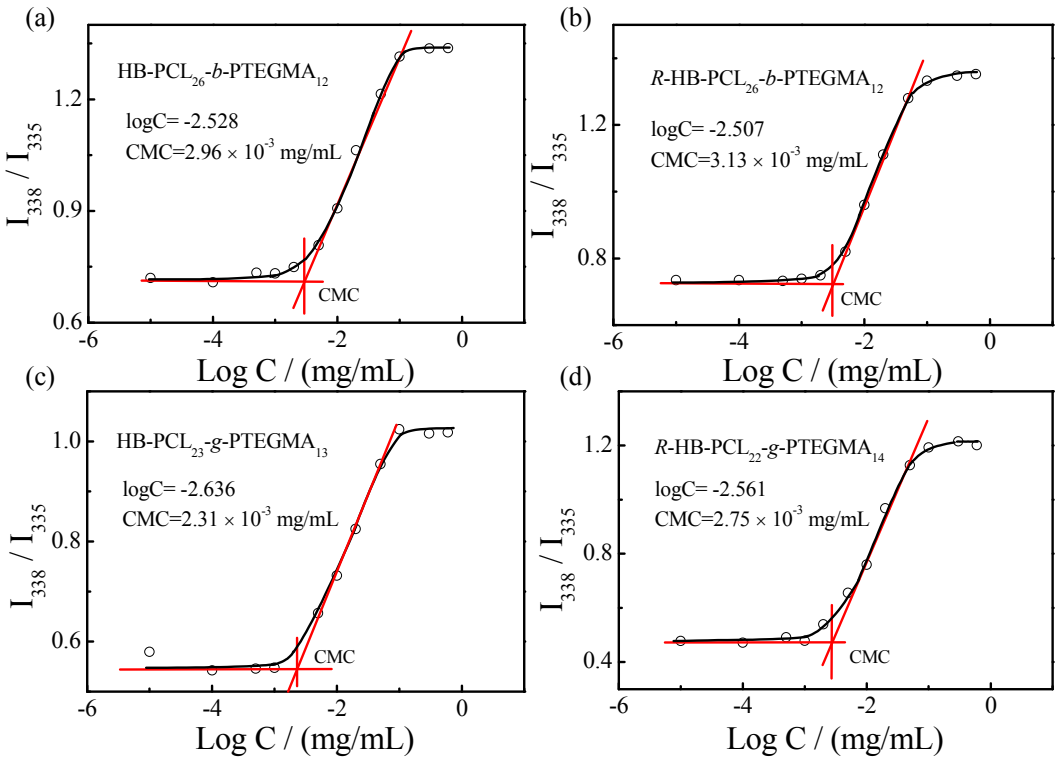

Figure S2. Plots of intensity ratio I_{338}/I_{335} from pyrene excitation spectra versus log C for (a) HB-PCL$_{26}$-*b*-PTEGMA$_{12}$, (b) *R*-HB-PCL$_{26}$-*b*-PTEGMA$_{12}$, (c) HB-PCL$_{23}$-*g*-PTEGMA$_{13}$, (d) *R*-HB-PCL$_{22}$-*g*-PTEGMA$_{14}$. Emission wavelength: 390 nm.

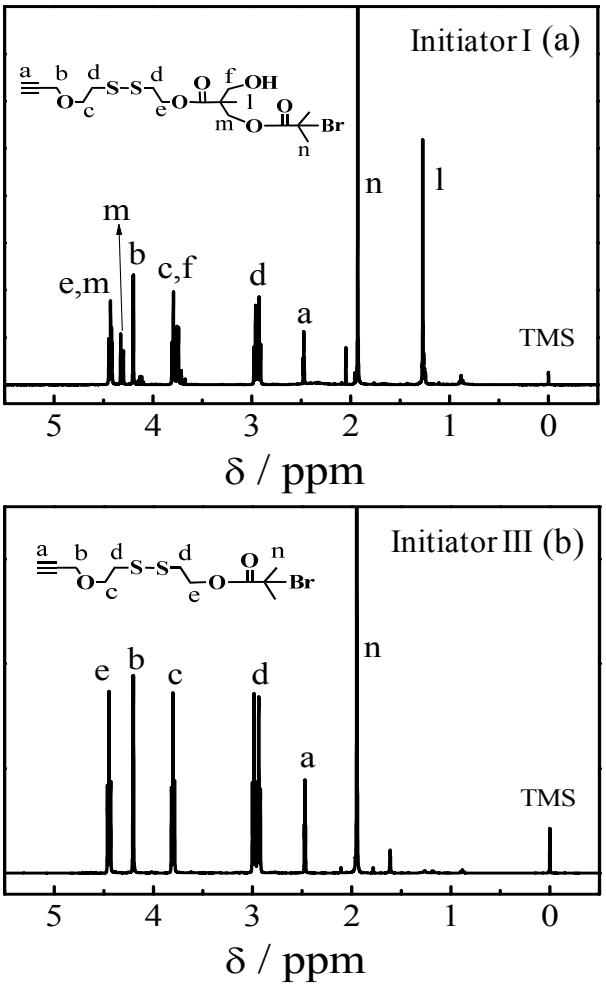

Figure S3. ^{1}H NMR spectra of (a) initiator I and (b) initiator III used in the main text.

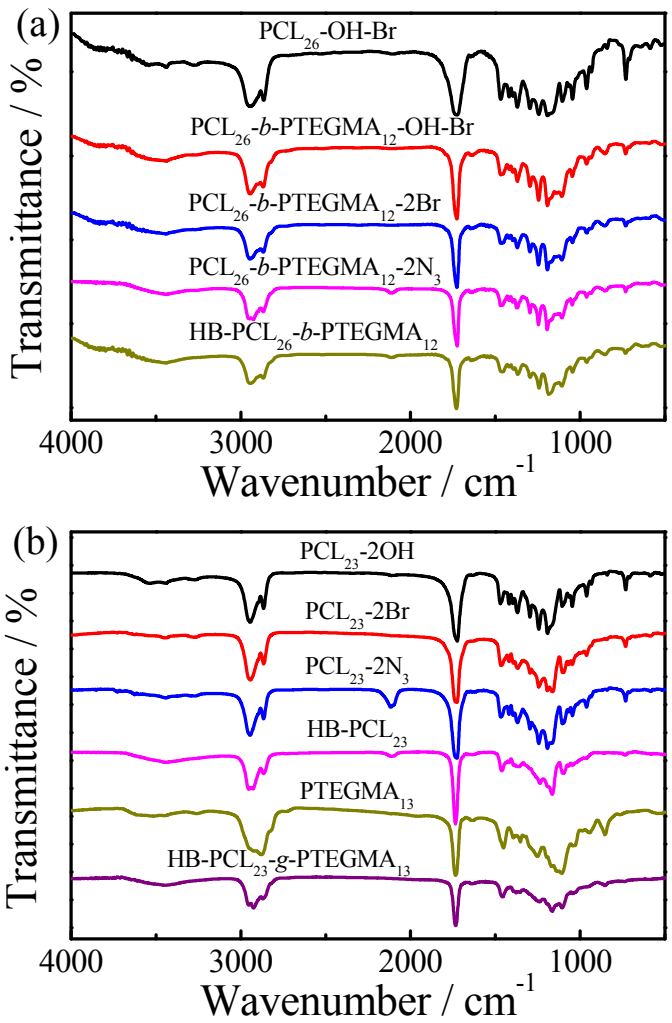

Figure S4. IR spectra of (a) the precursors and HB-PCL_{26}-*b*-$PTEGMA_{12}$, (b) the precursors and HB-PCL_{23}-*g*-$PTEGMA_{13}$.

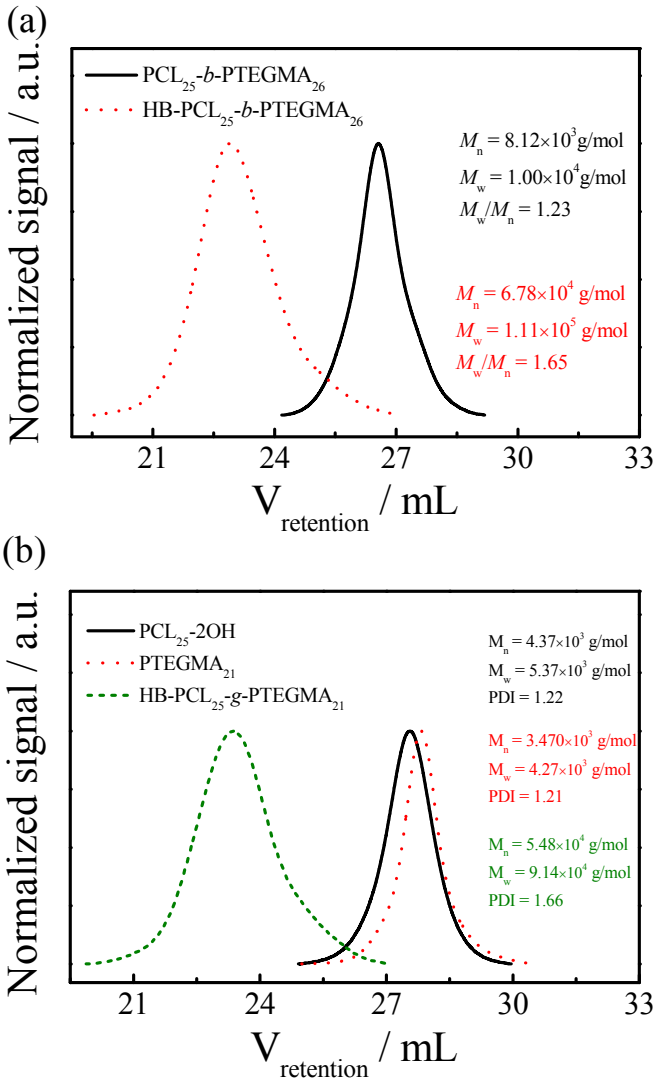

Figure S5. GPC curves of (a) the precursor and HB-PCL_{25}-*b*-$PTEGMA_{26}$, (b) the precursors and HB-PCL_{25}-*g*-$PTEGMA_{21}$ with disulfide linkages.

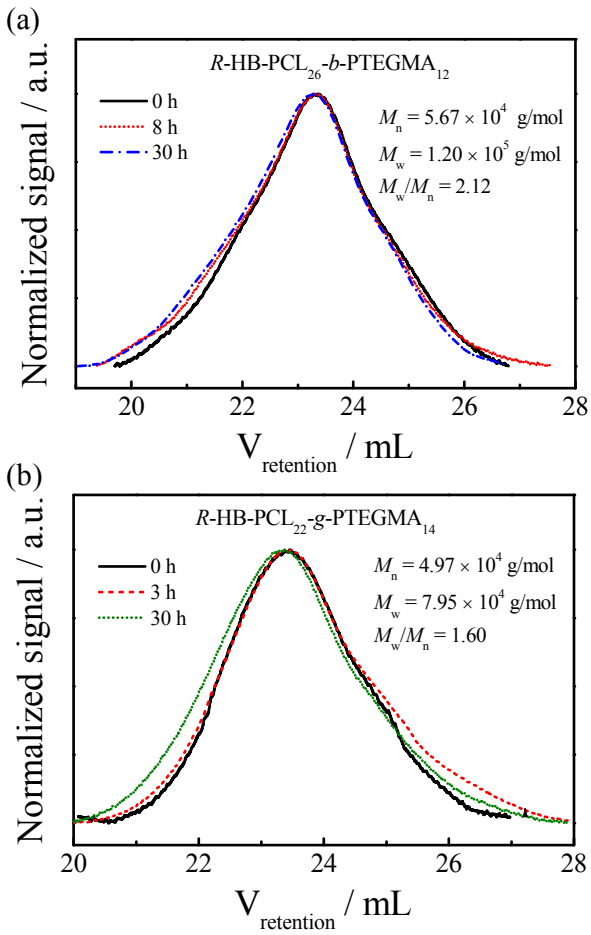

Figure S6. Evolution of GPC curves as a function of degradation time (t) for (a) R-HB-PCL$_{26}$-b-PTEGMA$_{12}$ and (b) R-HB-PCL$_{22}$-g-PTEGMA$_{14}$ without disulfide linkages, where [DTT] = 10 mM.

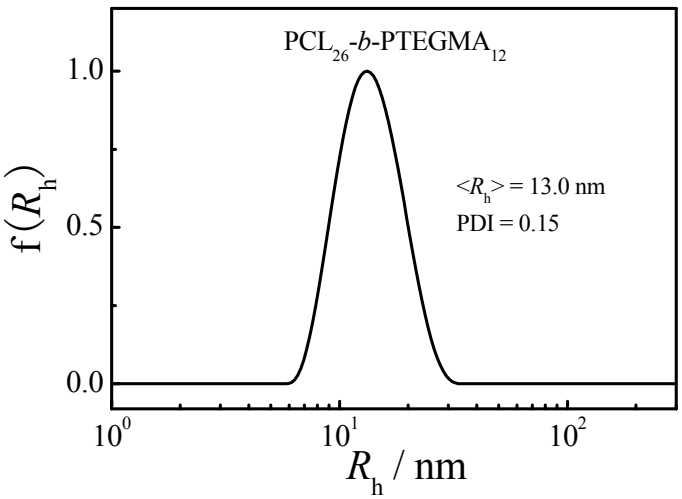

Figure S7. The hydrodynamic radius distribution $f(R_h)$ of the self-assembly amphiphiles formed from PCL$_{26}$-b-PTEGMA$_{12}$ diblock copolymer.

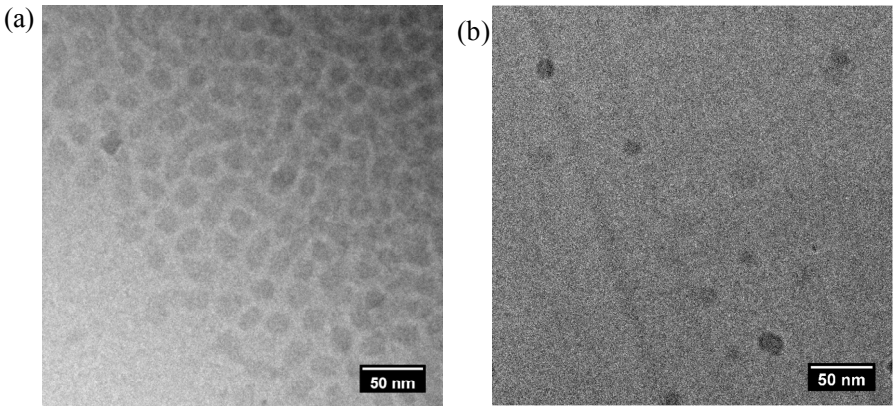

Figure S8. TEM micrographs taken from (a) HB-PCL$_{26}$-*b*-PTEGMA$_{12}$ SAs; (b) HB-PCL$_{26}$-*b*-PTEGMA$_{12}$ SAs after 24 h degradation in an aqueous phase (25 ^{o}C, 10 mM DTT). Transmission electron microscopy (TEM) was performed using a FEI T12 Quick CryoEM and CryoET microscope operated at 120 eV.

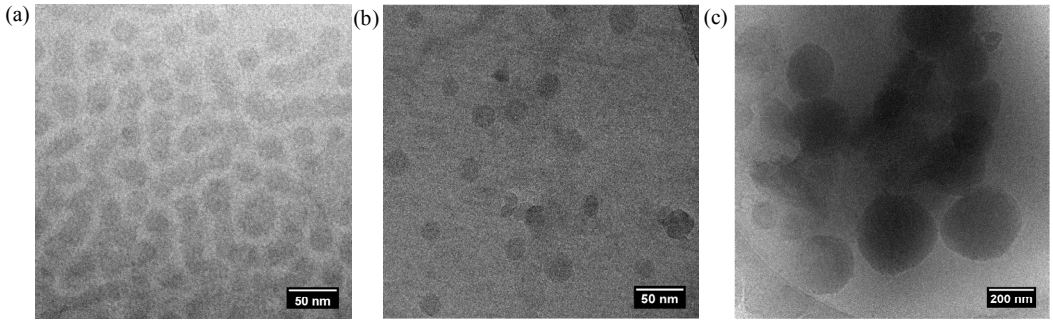

Figure S9. TEM micrographs taken from (a) HB-PCL$_{23}$-*g*-PTEGMA$_{13}$ SAs; (b) HB-PCL$_{23}$-*g*-PTEGMA$_{13}$ SAs after 24 h degradation; (c) HB-PCL$_{23}$-*g*-PTEGMA$_{13}$ SAs after 75 h degradation in an aqueous phase (25 ^{o}C, 10 mM DTT). Transmission electron microscopy (TEM) was performed using a FEI T12 Quick CryoEM and CryoET microscope operated at 120 eV.

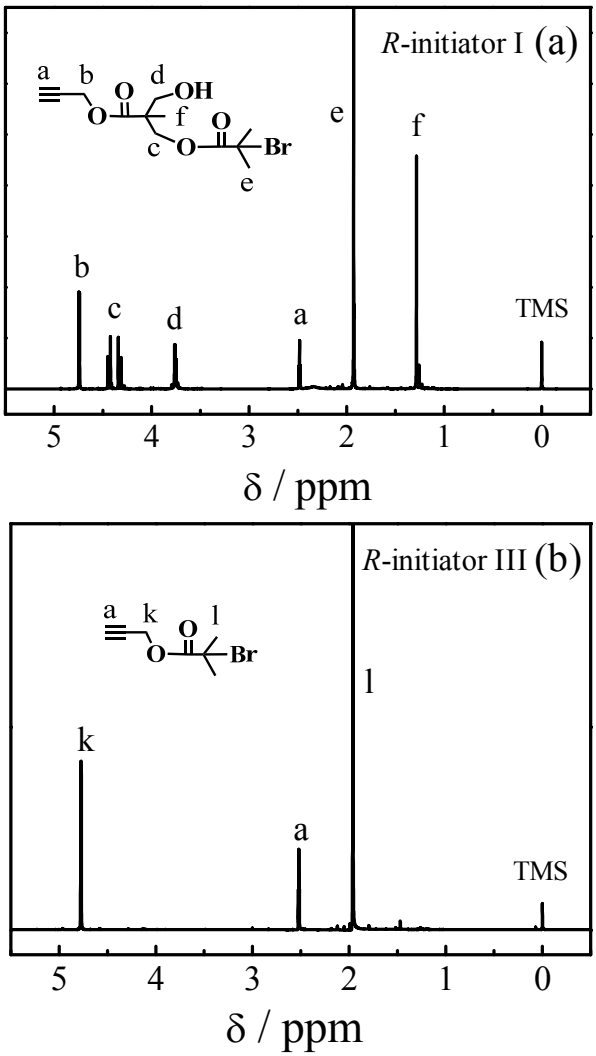

Figure S10. ^{1}H NMR spectra of (a) *R*-initiator I and (b) *R*-initiator III for reference samples.

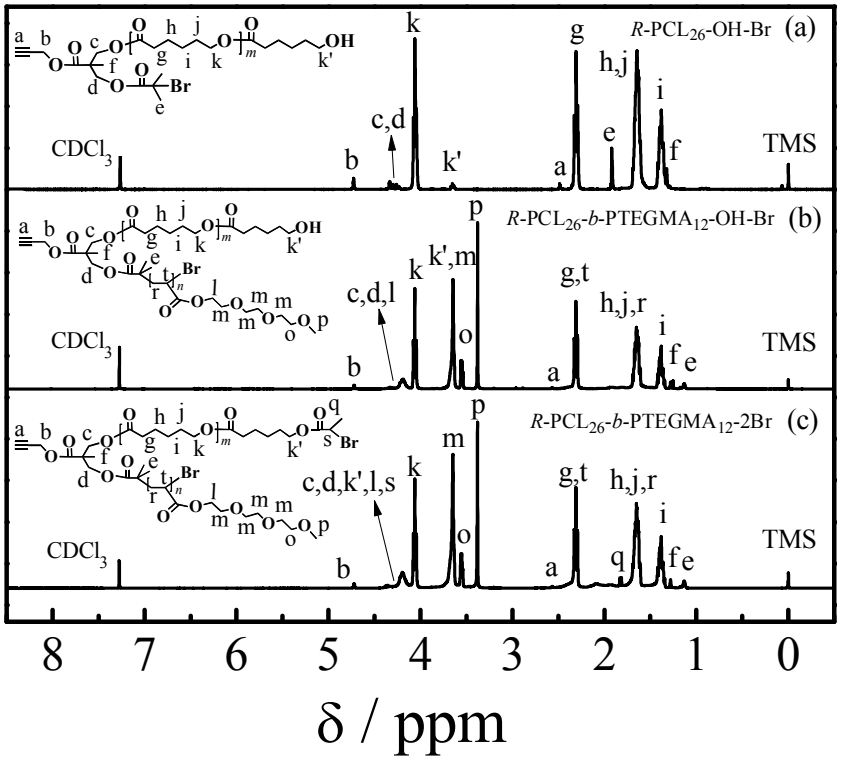

Figure S11. ^{1}H NMR spectra of (a) *R*-PCL$_{26}$-OH-Br; (b) *R*-PCL$_{26}$-*b*-PTEGMA$_{12}$-OH-Br; (c) *R*-PCL$_{26}$-*b*-PTEGMA$_{12}$-2Br without disulfide linkages.

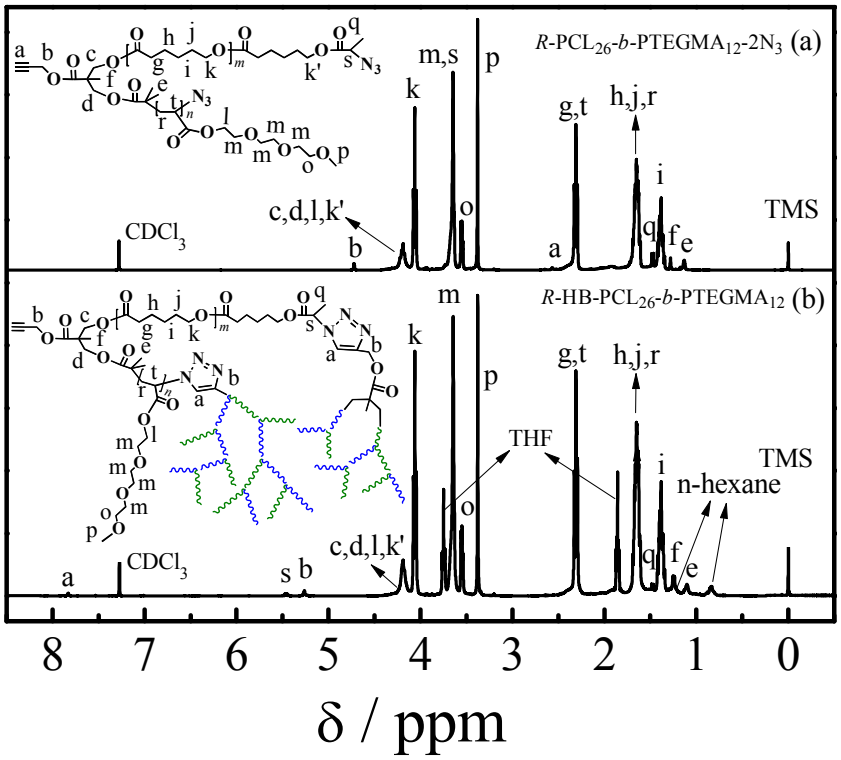

Figure S12. ^{1}H NMR spectra of (a) *R*-PCL$_{26}$-*b*-PTEGMA$_{12}$-2N$_3$, (b) *R*-HB-PCL$_{26}$-*b*-PTEGMA$_{12}$ without disulfide linkages.

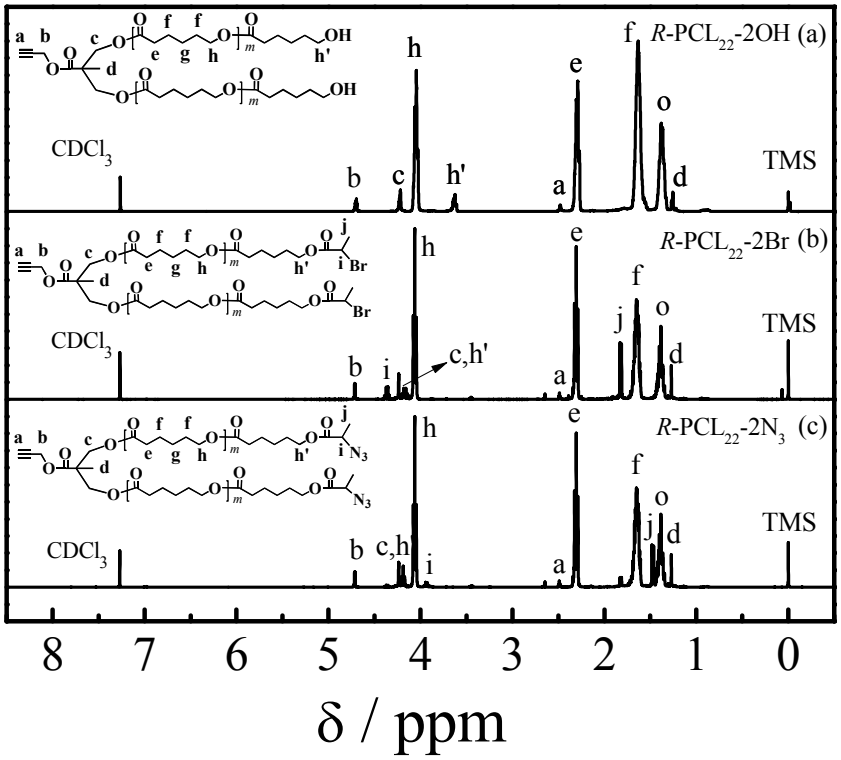

Figure S13. ^{1}H NMR spectra of (a) *R*-PCL$_{22}$-2OH, (b) *R*-PCL$_{22}$-2Br, (c) *R*-PCL$_{22}$-2N$_3$ without disulfide linkages.

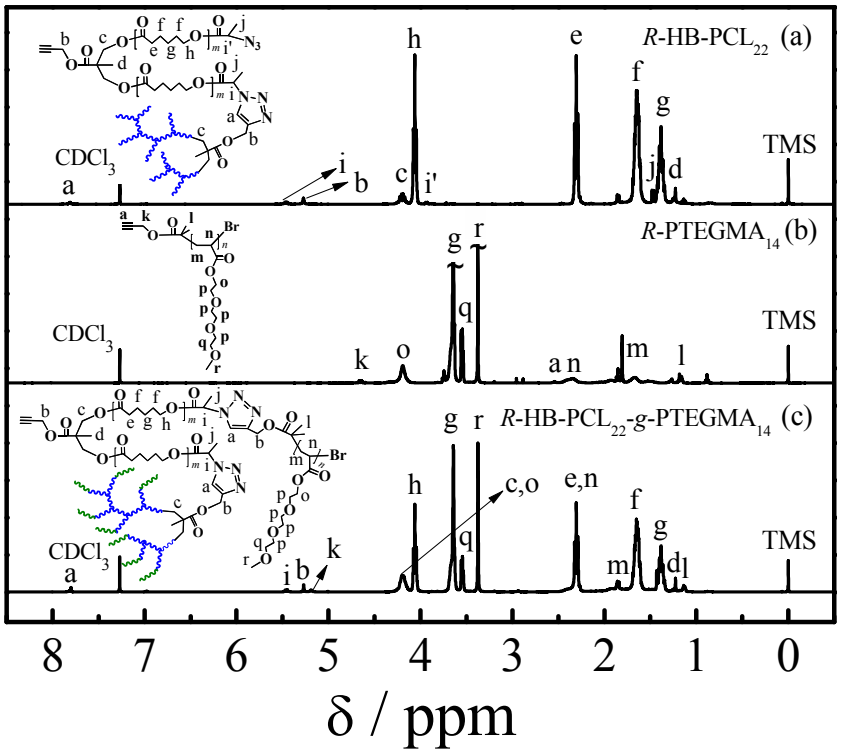

Figure S14. ^{1}H NMR spectra of (a) *R*-HB-PCL$_{22}$, (b) *R*-PTEGMA$_{14}$, and (c) *R*-HB-PCL$_{22}$-*g*-PTEGMA$_{14}$ without disulfide linkages.

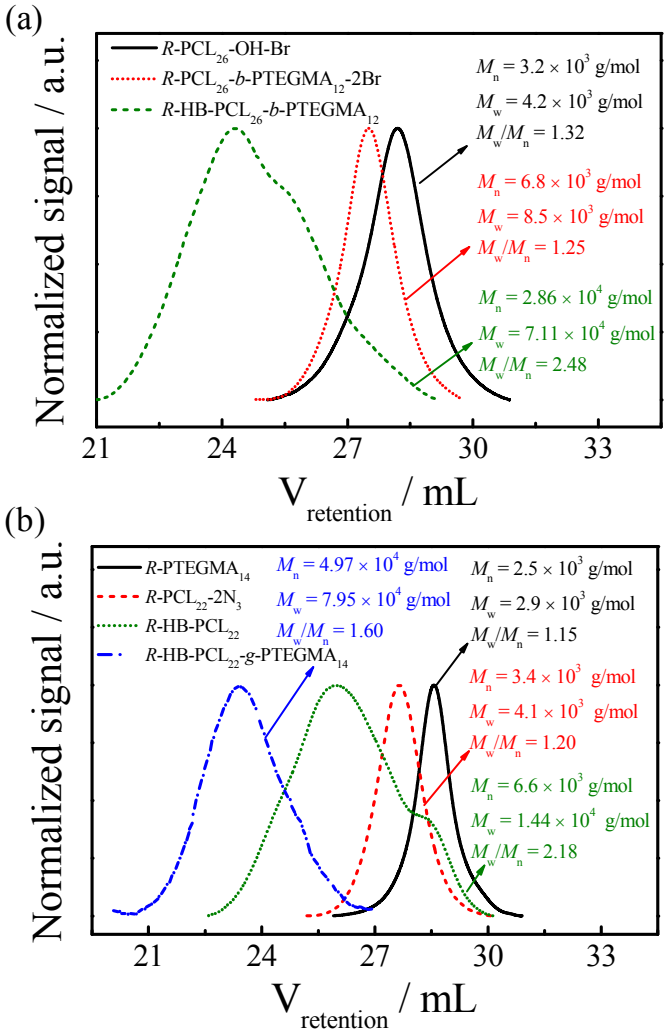

Figure S15. GPC curves of (a) the precursors and *R*-HB-PCL$_{26}$-*b*-PTEGMA$_{12}$, (b) the precursors and *R*-HB-PCL$_{22}$-*g*-PTEGMA$_{14}$ without disulfide linkages.

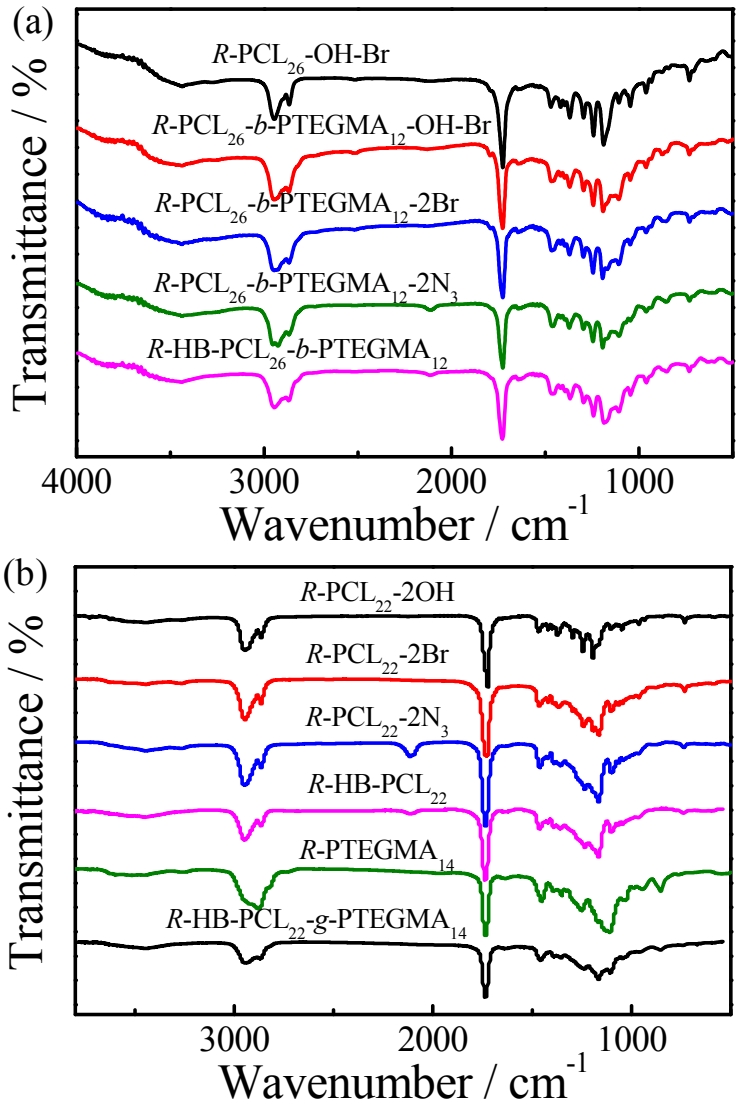

Figure S16. FTIR spectra of (a) the precursors and *R*-HB-PCL$_{26}$-*b*-PTEGMA$_{12}$, (b) the precursors and *R*-HB-PCL$_{22}$-*g*-PTEGMA$_{14}$ without disulfide linkages.

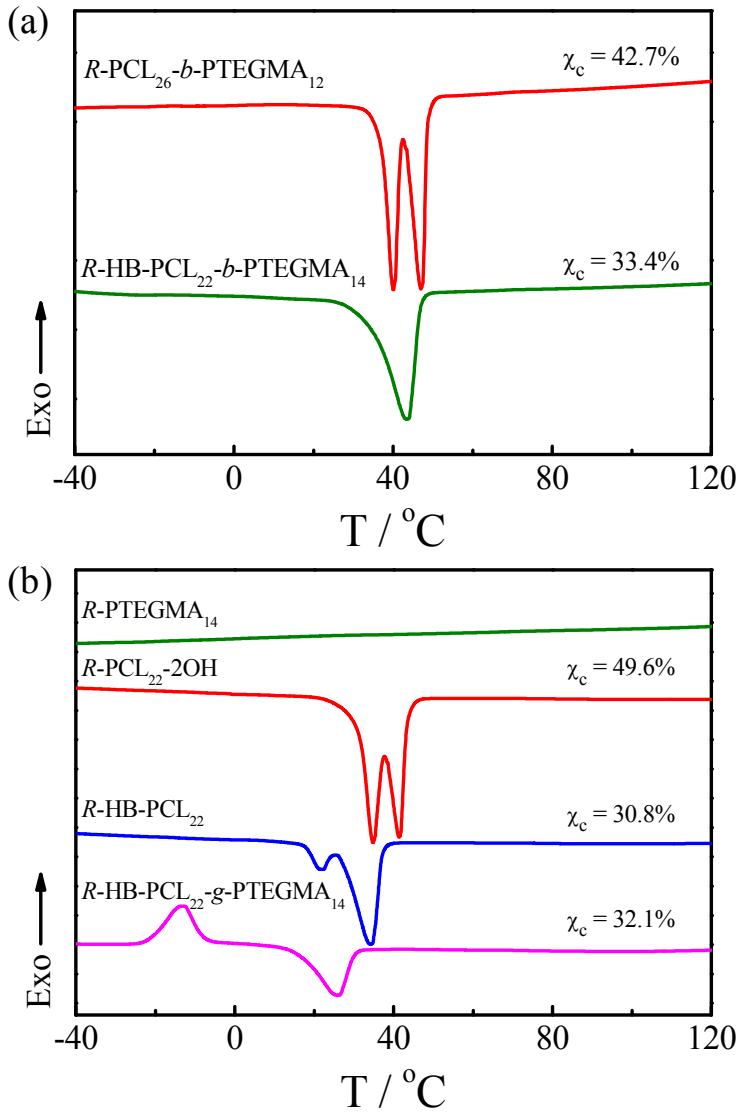

Figure S17. DSC curves (10 °C/min) during reheating of (a) the precursor and *R*-HB-PCL$_{26}$-*b*-PTEGMA$_{12}$, (b) the precursors and *R*-HB-PCL$_{22}$-*g*-PTEGMA$_{14}$ without disulfide linkages.

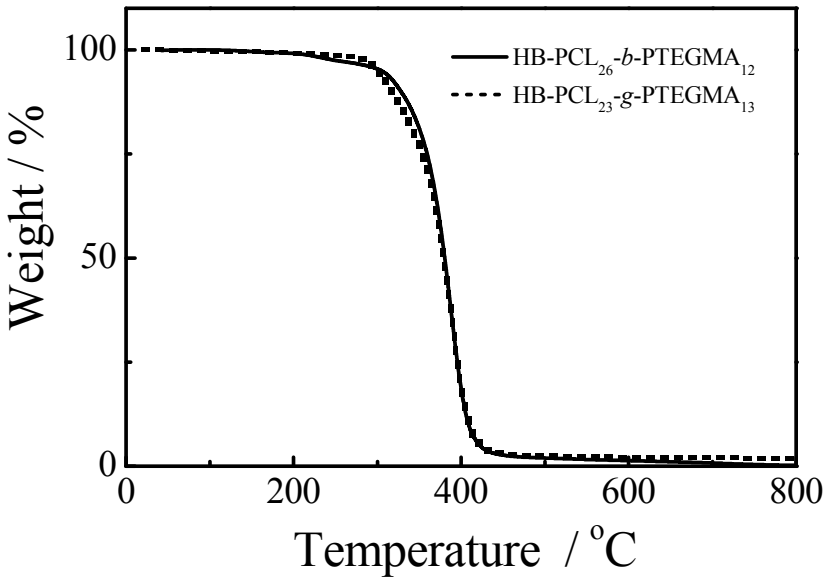

Figure S18. TGA curves of HB-PCL$_{26}$-*b*-PTEGMA$_{12}$ and HB-PCL$_{23}$-*g*-PTEGMA$_{13}$.

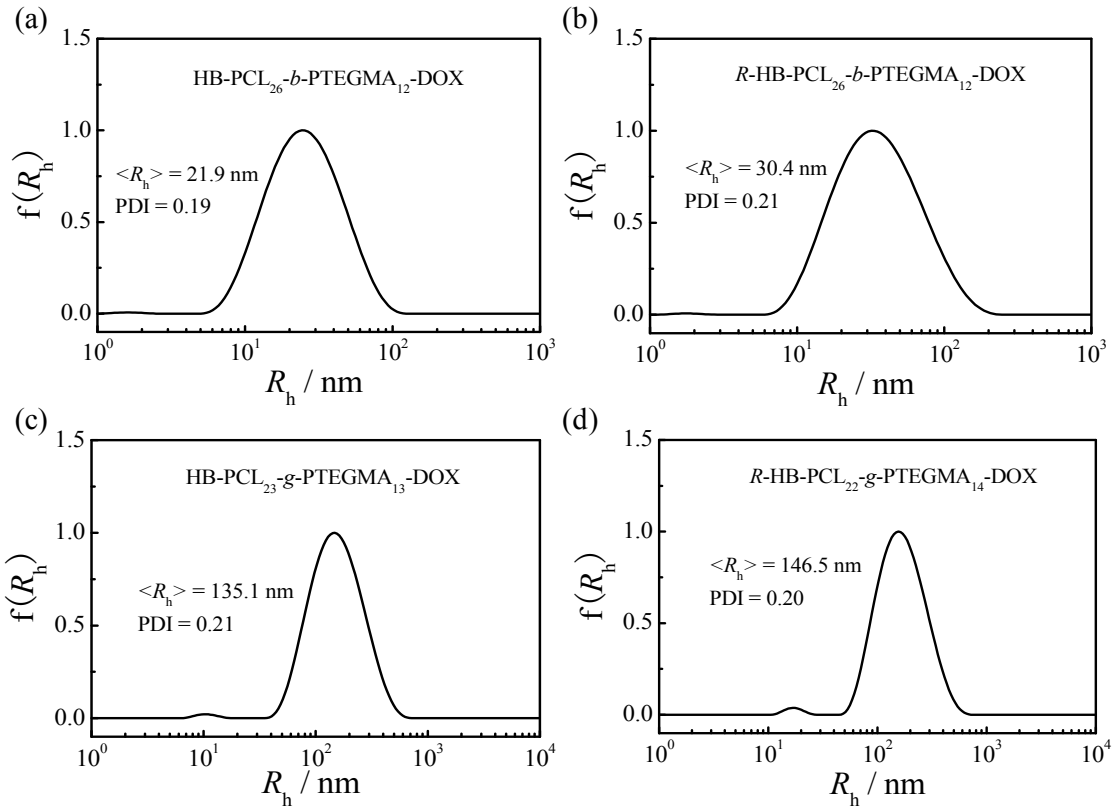

Figure S19. The hydrodynamic radius distribution $f(R_h)$ of DOX loaded self-assembly amphiphiles: (a) HB-PCL$_{26}$-*b*-PTEGMA$_{12}$-DOX, (b) *R*-HB-PCL$_{26}$-*b*-PTEGMA$_{12}$-DOX, (c) HB-PCL$_{23}$-*g*-PTEGMA$_{13}$-DOX, (d) *R*-HB-PCL$_{22}$-*g*-PTEGMA$_{14}$-DOX.

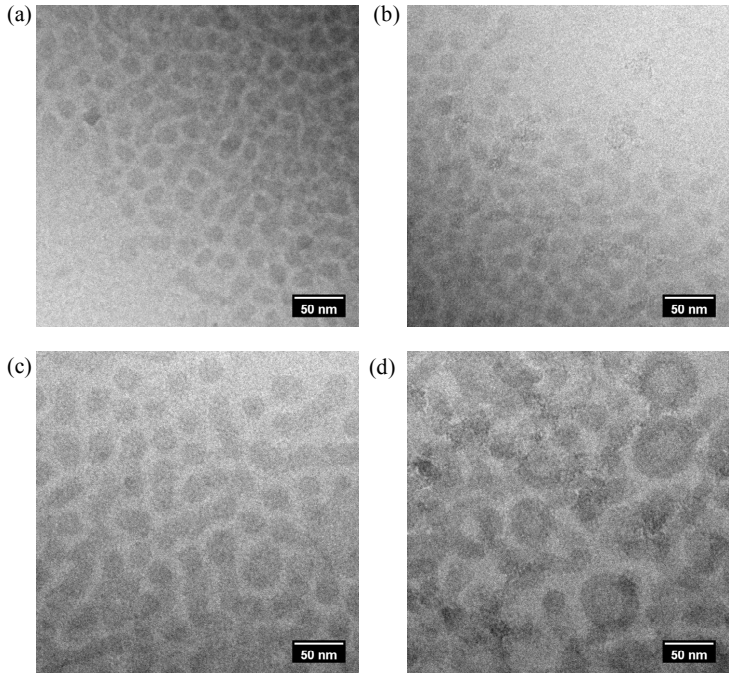

Figure S20. TEM micrographs taken from (a) HB-PCL$_{26}$-*b*-PTEGMA$_{12}$ SAs; (b) HB-PCL$_{26}$-*b*-PTEGMA$_{12}$-DOX SAs; (c) HB-PCL$_{23}$-*g*-PTEGMA$_{13}$ SAs and (d) HB-PCL$_{23}$-*g*-PTEGMA$_{13}$-DOX SAs. Transmission electron microscopy (TEM) was performed using a FEI T12 Quick CryoEM and CryoET microscope operated at 120 eV.

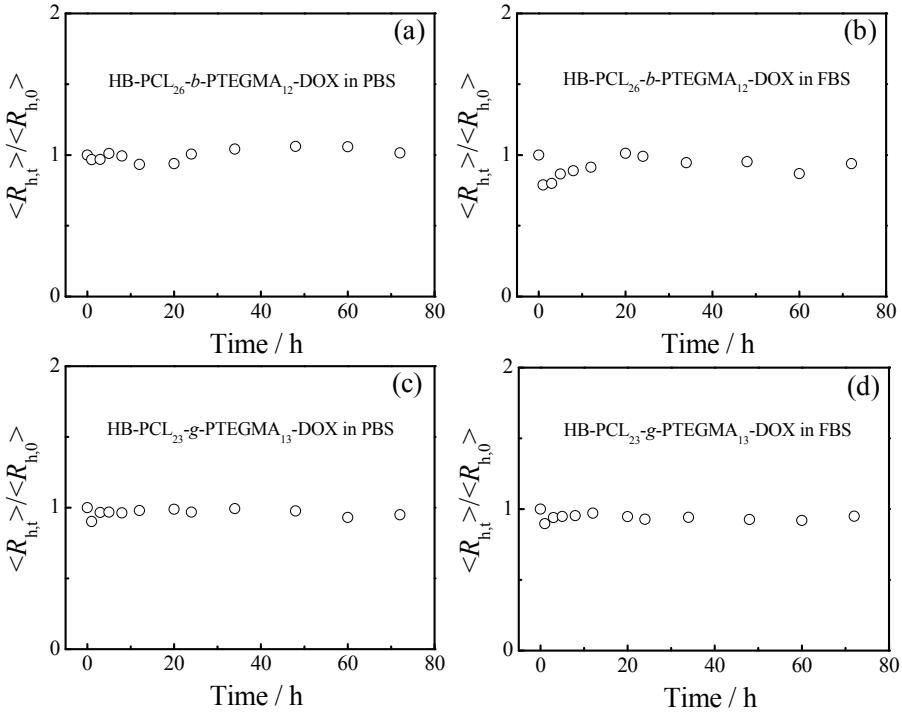

Figure S21. Time dependence of ratio ($<R_{h,t}>/<R_{h,0}>$) of average hydrodynamic radius at $t = t$ ($<R_{h,t}>$) and $t = 0$ ($<R_{h,0}>$) for HB-PCL$_{26}$-*b*-PTEGMA$_{12}$-DOX SAs in (a) PBS, (b) PBS containing 10% FBS; and HB-PCL$_{23}$-*g*-PTEGMA$_{13}$-DOX SAs in (c) PBS, (d) PBS containing 10% FBS at 37 ^{o}C.

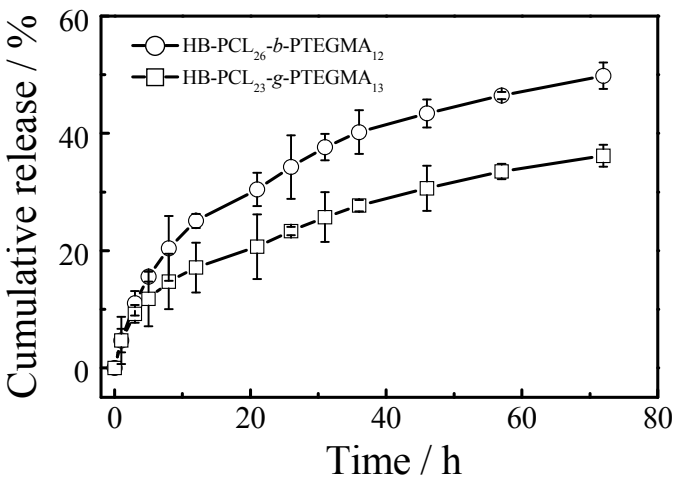

Figure S22. In vitro release of DOX from HB-PCL$_{26}$-*b*-PTEGMA$_{12}$-DOX and HB-PCL$_{23}$-*g*-PTEGMA$_{13}$-DOX SAs at 37 ^{o}C in 20 mM PB buffer (pH 7.4, 10 mM DTT).

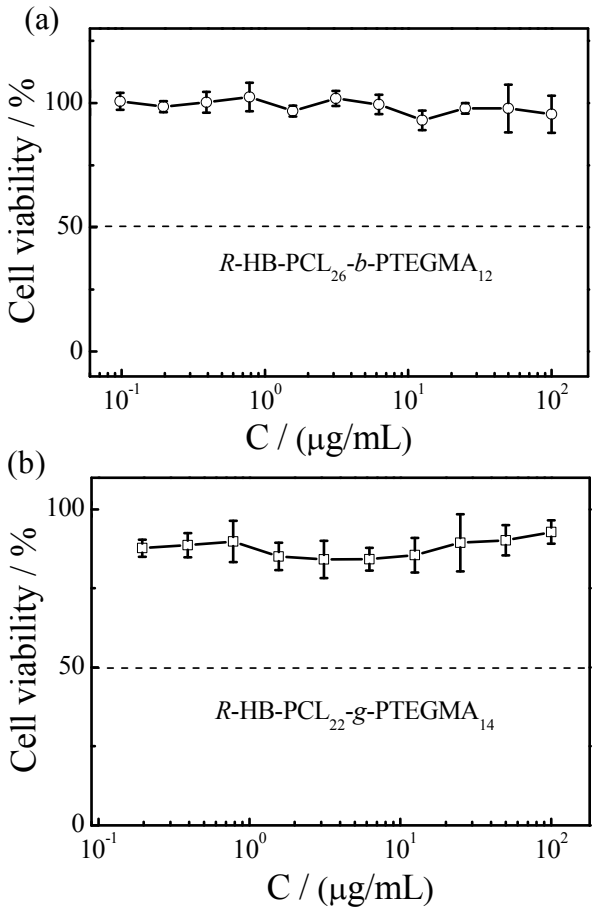

Figure S23. In vitro cytotoxicity of Hela cells against (a) bare *R*-HB-PCL$_{26}$-*b*-PTEGMA$_{12}$ self-assembly amphiphiles, (b) bare *R*-HB-PCL$_{22}$-*g*-PTEGMA$_{14}$ self-assembly amphiphiles without disulfide bonds for 48 h.

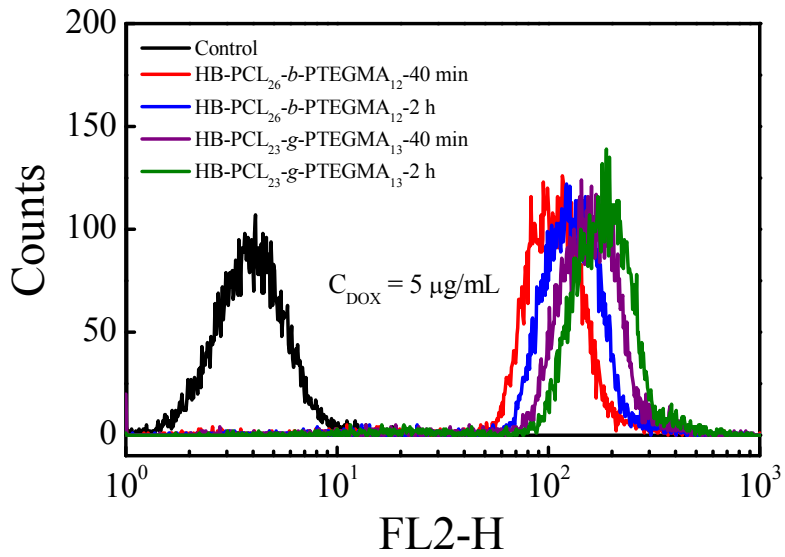

Figure S24. Flow cytometric analyses of HeLa cells after incubation (37 °C, 5% CO_2) with DOX-loaded Hyperbranched copolymer SAs.

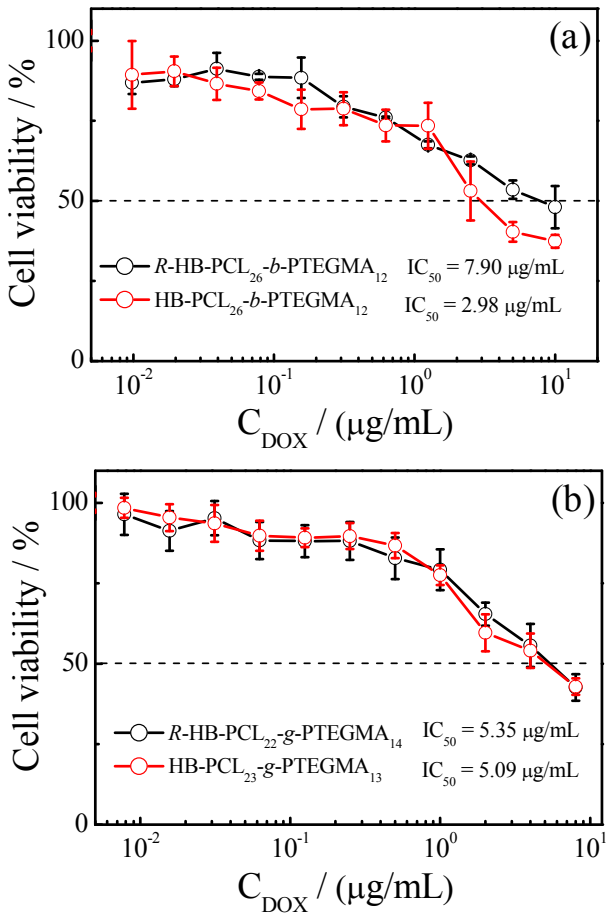

Figure S25. In vitro cytotoxicity of HeLa cells against (a) DOX loaded self-assembly amphiphiles of Hyperblock HB-PCL_{26}-*b*-$PTEGMA_{12}$ and *R*-HB-PCL_{26}-*b*-$PTEGMA_{12}$; (b) DOX loaded self-assembly amphiphiles of Hypergraft HB-PCL_{23}-*g*-$PTEGMA_{13}$ and *R*-HB-PCL_{22}-*g*-$PTEGMA_{14}$ for 48 h.